Ollila, S.T.T.; Denniston, C.; Ala-Nissilä, T.

One- and two-particle dynamics in microfluidic T-junctions

Published in:
Physical Review E

DOI:
10.1103/PhysRevE.87.050302

Published: 01/01/2013

Document Version
Publisher's PDF, also known as Version of record

Please cite the original version:
Ollila, S. T. T., Denniston, C., & Ala-Nissilä, T. (2013). One- and two-particle dynamics in microfluidic T-junctions. *Physical Review E*, *87*(5), 1-5. [050302]. https://doi.org/10.1103/PhysRevE.87.050302

PHYSICAL REVIEW E **87**, 050302(R) (2013)

One- and two-particle dynamics in microfluidic T-junctions

Santtu T. T. Ollila,[1,2,*] Colin Denniston,[2,†] and Tapio Ala-Nissila[1,3,‡]

[1]*COMP Centre of Excellence, Department of Applied Physics, Aalto University School of Science and Technology, P.O. Box 11000, FIN-00076 Aalto, Espoo, Finland*

[2]*Department of Applied Mathematics, University of Western Ontario, London, Ontario N6A 5B8, Canada*

[3]*Department of Physics, Brown University, Providence, Rhode Island 02912-1843, USA*

(Received 2 March 2013; published 30 May 2013)

Advances in precise focusing of colloidal particles in microfluidic systems open up the possibility of using microfluidic junctions for particle separation and filtering applications. We present a comprehensive numerical study of the dynamics of solid and porous microparticles in T-shaped junctions. Good agreement with experimental data is obtained on the location of particle-separating streamlines for single solid particles with realistic parameters corresponding to the experiments. We quantify the changes in the position of the separating line for porous, partially penetrable colloids. A prediction of the full phase diagram for particle separation is presented in the case of two successive particles entering a T-junction. Our results suggest the intriguing possibility of using the one- and two-particle T-junctions as logic gates.

DOI: 10.1103/PhysRevE.87.050302 PACS number(s): 83.10.Rs, 47.57.−s, 47.85.L−, 82.70.Dd

The ability to routinely engineer high-quality microfluidic networks has made it possible to take advantage of well-established physical phenomena such as inertial separation [1–3] only found in confined systems and apply them to ordering [4] and filtration of particles based on their size [5] and shape [6]. Continuous blood plasma separation has been realized experimentally using simple microfluidic devices [7,8]. Precise focusing of particle streams has been demonstrated experimentally [9,10], which serves as motivation for more complicated forms of automated transport.

A fundamental building block in microfluidic circuits is the T-shaped junction with one inlet and two outlets as illustrated in Fig. 1. An interesting case is where there is a flow asymmetry between outlets 1 and 2 such that, while the flow rates satisfy the conservation law $Q_0 = Q_1 + Q_2$, the outflow rates are such that $Q_1 < Q_2$. Such an asymmetric flow can be generated in the T-channel by controlling the pressure difference between the two outlets. The relevant question is what happens to colloidal particles, which are released in the inlet at some distance D_0 away from the T-junction, and which deviate by a distance s from the center of the inlet. Experimentally, Svanes and Zweifach [11] and Fung [12] were the first to observe for red cells that $N_1/N_0 < Q_1/Q_0$; i.e., the fraction of red cells, N_1/N_0, entering the low-flow-rate branch is smaller than the proportion of solvent, Q_1/Q_0, going there. More recently, Doyeux *et al.* [9] investigated the physics behind the Zweifach-Fung effect. They concluded that the decrease in the particle fraction in the low-flow-rate branch is mainly due to the distribution of particle position in the inlet and that particle trajectories do not track the streamlines of the undisturbed flow.

To use microfluidic T-junctions in medical and engineering applications requires understanding how particles of different mechanical properties (mass distribution, porosity, size, and shape) move through an asymmetric T-junction, i.e., how they are split between the two outlets with given initial conditions and mechanical properties. One important physical parameter of focus is the particle porosity. For example, large porous particles have been demonstrated to function as carriers of medical nanoparticles in drug delivery with particularly promising results in their sustained delivery in the lungs [13]. They are able to escape the lungs' natural clearance mechanisms until the medical payload is delivered [14].

In this Rapid Communication, our aim is to map out the single- and two-particle dynamics in asymmetric T-junctions using a recently developed lattice-Boltzmann-based simulation technique for extended solid and porous particles [15–17]. We first demonstrate that our model agrees quantitatively with experiments [9] in terms of the outlet distributions of fluid and impermeable, solid particles in a T-junction. Based on this we explain how it enables filtration of particles by size or by porosity. In order to consider particle-particle interactions, we map out a two-particle phase diagram of particle distribution in the outlets as a function of their inlet distribution. We also demonstrate that unequal flow rates in the outlets could be used to realize operations of binary logic by focusing particles in the inlet. For a fixed degree of flow asymmetry, we demonstrate a two-particle NAND and a one-particle NOT gate, whose underlying physics is explained by the phase diagram of two-particle flow in the system. Microfluidic channels have been previously proposed as building blocks of a microfluidic computer [18]. Our work raises the intriguing possibility of using microfluidic T-junctions as logic gates to build such a device.

Theory. For the problem at hand, we need an accurate determination of the hydrodynamic forces and torques on the colloidal particles. This is achieved by modeling the solvent using the incompressible Navier-Stokes equation,

$$\nabla \cdot \mathbf{u} = 0, \quad \rho\,(\partial_t \mathbf{u} + \mathbf{u} \cdot \nabla \mathbf{u}) = \eta \nabla^2 \mathbf{u} - \nabla p + \mathbf{f}, \qquad (1)$$

where ρ is the constant fluid mass density, $\mathbf{u}$ is the fluid velocity, η is the shear viscosity, and p is the pressure. The

*santtu.ollila@aalto.fi
†cdennist@uwo.ca
‡tapio.ala-nissila@aalto.fi

porous particle is present as a force density $\mathbf{f}$,

$$\mathbf{f} = \gamma n(\mathbf{r})(\mathbf{v} - \mathbf{u}), \quad n(\mathbf{r}) = \begin{cases} \lambda, & \mathbf{r} \in B(t), \\ 0, & \mathbf{r} \notin B(t), \end{cases} \tag{2}$$

where the coupling constant γ has units of mass per time and $\mathbf{v}$ is the local velocity of the particle, which contains contributions from center-of-mass and rotational motion. In the absence of the nonlinear term, Eqs. (1) and (2) are the Debye-Bueche-Brinkman (DBB) model [15,19–22], which is suitable for our purposes as it allows one to study generic hydrodynamic effects between a solvent and uniformly porous particles with few parameters.

The "node" density $n(\mathbf{r})$ has units of inverse volume and has a constant value λ inside the volume $B(t)$ of the particle and zero outside of it. Inside $B(t)$, the fluid flow is perturbed by the nodes. The shape $B(t)$ can be varied to give a shell or other desired mass distribution [15]. The degree of permeability for a spherical particle is conveniently given by the dimensionless number $\beta \equiv R\sqrt{\gamma\lambda/\eta}$. As is typically done, we assume the viscosity to be η both inside and outside of $B(t)$. The γ-dependent force and torque on the particle are given by Newton's third law through integration of $-\mathbf{f}$ and $(\mathbf{r} - \mathbf{r}_{\rm cm}) \times (-\mathbf{f})$ over $B(t)$.

Model. The system (Fig. 1) has a single inlet with a fluid influx of Q_0 (mass per unit time) and outlets 1 and 2 such that $Q_0(t) = Q_1(t) + Q_2(t)$. We impose no-slip boundary conditions (BCs) at the sidewalls [24] and Poiseuille velocity profiles at the inlet and at the outlets, which are set based on the respective rates of mass flux. To remove reflections, the open boundaries are impedance-matched by requiring

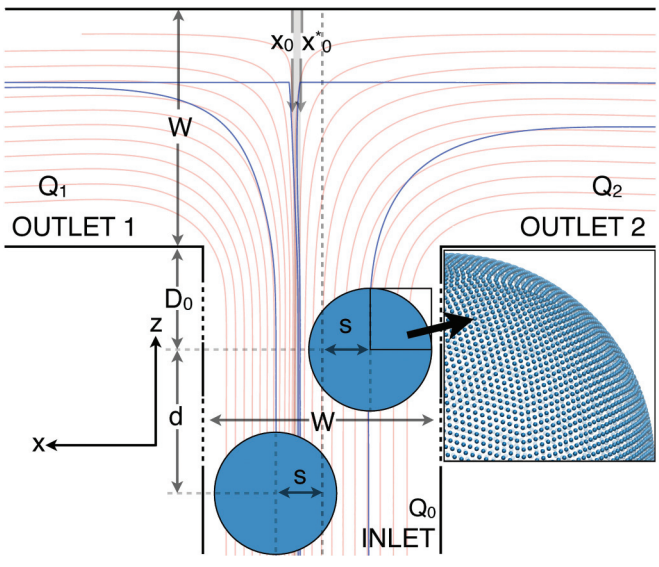

FIG. 1. (Color online) Two cases of a particle approaching the bifurcation offset by s from the centerline and entering one of the outlets. In its absence, the solvent flows leftward (rightward) when located at $x > x_0$ ($x < x_0$). A particle flows leftward (rightward) when started at $x > x_0^*$ ($x < x_0^*$). Within the narrow gray region ($x_0 > x > x_0^*$), solvent flows rightward and a particle leftward (see text). x_0 and x_0^* are functions of Q_1/Q_0. Streamlines are sketched for $Q_1/Q_0 = 0.35$ (red or light gray) and a few single-particle trajectories are also shown (blue or dark gray). The nodal structure (generated with the VMD software [23]) of the shell is shown on the right.

$(\hat{\mathbf{n}} \cdot \nabla)^2 p = 0$, where $\hat{\mathbf{n}}$ is a unit vector normal to the open boundary. All branches are long enough so that the BCs have no effect on the flow field in the vicinity of the bifurcation. The condition on the second derivative of p is imposed on the local density using three-point finite differences as $p \propto \rho$ [25]. Experimentally, the pressure differences are controlled by changing the relative hydrostatic pressures [9].

The DBB model can be solved analytically in some steady states and for an oscillating particle [15]. However, walls and other particles make the model intractable analytically, which is why we use a lattice-Boltzmann (LB) [26] algorithm to solve Eq. (1) numerically instead. Our model [15–17] reproduces the compressible Navier-Stokes equations [27,28] with DBB-like forces, and we have validated it against theoretical results [15]. Here, we use the shear viscosity $\eta = 0.01\ \mathrm{g\,cm^{-1}\,s^{-1}}$ and density of water, $\rho = 1\ \mathrm{g\,cm^{-3}}$. Our porous shell is represented by a rigid surface triangulated with N nodes (Fig. 1 inset), which couple to the LB fluid through local interpolation [15–17,29]. Importantly, γ and N are calibrated to values that guarantee consistency between different measurements of the particle's hydrodynamic radius for a given degree of porosity [15,17]. N corresponds to a node placement denser than the resolution Δx of the underlying cubic fluid lattice; i.e., $\langle n(\mathbf{r})\rangle > \Delta x^{-3}$.

To prevent overlaps, each node interacts with those on other colloids and walls purely repulsively through a truncated and shifted 12-6 Lennard-Jones (LJ) potential with parameters set to approximate hard spheres. Varying the LJ energy scale (ϵ) in the colloid-colloid interaction over four decades does not change the two-particle results as the dynamics are dominated by hydrodynamic interactions. The physical dimensions of the system were similar to recent experiments [9]: the width of all branches is set to $W = 60\ \mu$m (see Fig. 1). Unless otherwise noted, the flow rate at the inlet is $Q_0 = 0.021\ \mathrm{mg\,s^{-1}}$, giving a maximum solvent velocity of $u_{\rm max} = 0.085\ \mathrm{mm\,s^{-1}}$. These numbers give $\mathrm{Re} \equiv \rho W u_{\rm max}/\eta \approx 0.53$. We study a variant of the problem in which the system is periodic in the y direction with a depth slightly greater than the channel width. Computation is done in units of the lattice discretization $\Delta x = 2.0\ \mu$m and $\Delta t = 0.53\ \mu$s. Thermal fluctuations can be neglected for these parameters.

Results. We have reproduced the experimental results of Doyeux *et al.* (Fig. 5 in Ref. [9]) in the limit of impermeable particles using our model. That is, we have computed the positions of the fluid (x_0) and particle-separating (x_0^*) streamlines. These coordinates determine in which outlet fluid (left: $x > x_0$, right: $x_0 > x$) and a colloid particle (left: $x > x_0^*$, right: $x_0^* > x$) end up as a function of the fraction Q_1/Q_0 of fluid entering branch number 1 on the left in Fig. 1. The ratio Q_1/Q_0 can be controlled precisely by adjusting the pressure BC at the open boundaries. With no loss of generality, we consider only $Q_1/Q_0 \leqslant 1/2$. The coordinate x_0 can easily be calculated in the inlet far from the junction for an incompressible fluid from

$$Q_1/Q_0 = \int_0^{x_0} u_z(x)\,dx \Big/ \int_0^{W} u_z(x)\,dx, \tag{3}$$

where $u_z(x)$ is the Poiseuille flow velocity. Interestingly, x_0 does not in general equal x_0^* in the bifurcation. We find $x_0 \geqslant x_0^*$

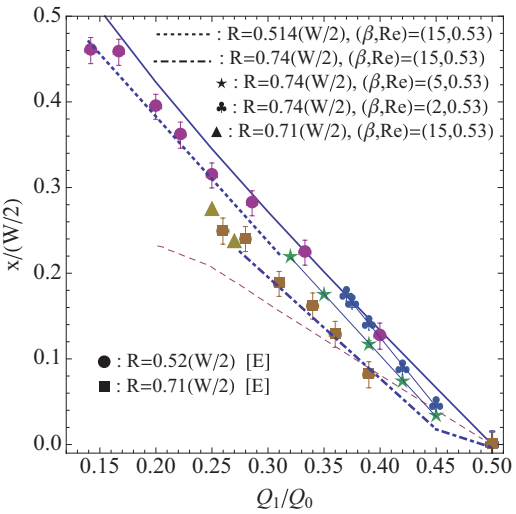

FIG. 2. (Color online) Location of the fluid (x_0, thick solid line) and the particle separating (x_0^*, dotted and dot-dashed lines, symbols) coordinate as a function of the fraction of fluid exiting through outlet 1 for different particle radii (R) and levels of porosity (β). Data below x_0 indicate that x_0^* is located rightward of x_0 in Fig. 1. With decreasing Q_1/Q_0, x_0 and x_0^* move leftward. Our theoretical model (dotted and dot-dashed lines) agrees with experimental "[E]" results [9] (● and ■). The more porous the particle is (dot-dashed line, ★, ♣) the farther left it needs to reside in the inlet for it to exit through outlet 1. Comparing Doyeux and coworkers' two-dimensional model (dashed line) to their experiments indicates that a full three-dimensional description (our model, dot-dashed line) is needed to account for the experiments.

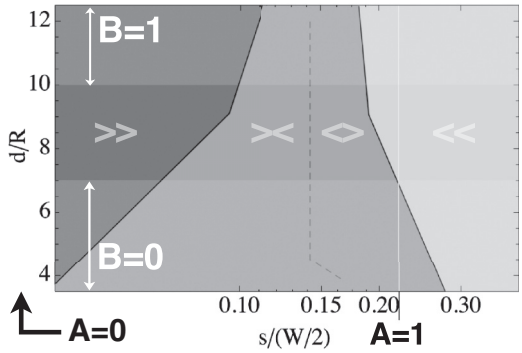

FIG. 3. Phase diagram of two-particle flow as a function of initial separation d/R ($2R = 0.514W$ and $\beta = 10$) and normalized offset to the left of the centerline $s/(W/2)$ at $Q_1/Q_0 = 3/8$. The solid lines separate different phases and the markings indicate the branches entered by the particles. For example, <> tells us the first particle went left (<) and the second particle went right (>). The mass flux in the inlet corresponds to Re = 5.3. The values attributed to the binary variables A and B (see text) are indicated as well. The vertical dashed line is the phase boundary between > and < in single-particle flow (cf. Fig. 2), and including the tilt at $d/R = 4$ it is the phase boundary between >< and <>, too.

for $\beta = 15$ (essentially an impermeable case), which means the particle need not be offset as much to the left as a fluid element for it to enter the low-flow-rate branch. We found our numerical values of x_0 to agree very well with the analytical solution to Eq. (3) as $\rho(\mathbf{r})$ is constant for a fixed x in the inlet. Our findings for x_0 and x_0^* are plotted in Fig. 2 together with the data of Doyeux *et al.* [9]. The agreement between their measurements for polystyrene particles of $2R/W = 0.71$ (■) at Re ≈ 0.1 and our simulations for $2R/W = 0.743$ and $\beta = 15$ (dot-dashed line) at Re $= 0.53$ is good. In fact, the simulation data for $2R/W = 0.71$ and 0.743 are indistinguishable for $0.28 < Q_1/Q_0 < 0.45$. However, because our particle $[R/(W/2) = 0.743]$ is larger than Doyeux's (0.71), its maximal hard-sphere offset $s_{\max}/(W/2) = 1 - R/(W/2) \approx 0.257$ toward the wall is smaller than $s_{\max} = 1 - 0.71 = 0.29$ for Doyeux's. Our data for $R/(W/2) = 0.71$ match the experiments (■) for $Q_1/Q_0 < 0.275$.

As the level of porosity is increased (β decreases), x_0^* moves leftward, closer to x_0 and toward the low-flow-rate outlet, which is seen as a shift in the particle-separating streamline position and an increase in the slope for $2R = 0.74W$ in Fig. 2 as β goes from 15 to 5 to 2. Such propensity for a sensitized Zweifach-Fung effect can be used for porosity-based filtration at a fixed offset s where impermeable particles (large β) move leftward and more permeable particles rightward. Similarly, filtration based on radius (e.g., $2R/W = 0.514$ and 0.74) is achieved by focusing particles onto, for example, the coordinate $x/(W/2) = 0.22$ at a fixed asymmetry of $Q_1/Q_0 = 0.3$, which results in large particles ($2R = 0.74W$) moving leftward and small ones moving rightward ($2R = 0.514W$).

Focusing devices such as those of Refs. [9,10] operate on streams of particles for which reason one must consider interactions of particles as they move through the T-junction. This is why it is crucial to understand the *joint* phase diagram of the bifurcation of the particles when they traverse an asymmetrically driven T-junction. We have determined such two-particle phase diagrams, which describe how the two successive particles bifurcate between the outlets 1 and 2 as a function of their mutual offset, $s/(W/2)$, and interparticle separation, d/R. Such diagrams can be viewed as first-order corrections to the data of Fig. 2, which are recovered theoretically in the limit $d/R \to \infty$. Figure 3 shows a typical diagram at $Q_1/Q_0 = 3/8$ for particles offset left of the inlet's centerline. The data were acquired for a given integer-valued d/R by iteration. First, two values of the common offset s were found, which gave different two-particle outcomes (e.g., both went leftward and one in each branch). The midpoint of the two was then used to narrow in on the precise location of the phase boundary until an uncertainty of 0.05 R was reached. For $Q_1/Q_0 \in [1/4,3/8]$, the diagram has three distinct phases: both particles move leftward (≪), rightward (≫), or in different directions (<> or ><). The mechanism leading to <> and >< is an intermediate $|s|$ and small separation d for which the first particle enters and temporarily partially blocks a branch, during which time the trailing particle traverses the junction and enters the other branch. The ≪ and ≫ entries occur when $|s|$ is either large enough that both particles are well into the region where they both follow the streamlines out or that they are far enough apart (large d) so that they essentially follow the single-particle case.

The precise experimental control of the positions of the colloidal particles in microfluidic channels opens up the intriguing possibility to use structures such as the T-junctions as logic gates. We fix Q_1/Q_0 to 0.375 and β to 10 from here on,

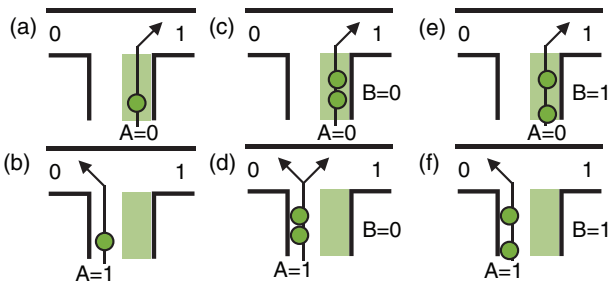

FIG. 4. (Color online) The operational basis of a single-particle NOT gate [(a) and (b)] and a two-particle NAND gate [(c)–(f)] for $\beta = 10$ particles in terms of variables A and B (see text and Fig. 3).

where the latter choice results in weakly permeable particles [15]. Many colloids of biological origin have a permeable outer surface, which should make these results relevant to biological systems, too. For example, the fundamental NOT gate is realizable for the single-particle flow if we assign the binary outcome 0 for the left and 1 for the right branch, and we define the binary variable A as $A = 0$: $s/(W/2) < 0$, $A = 1$: $s/(W/2) = 0.22$. A more general condition would work for a NOT gate, but we pick 0.22 as it will be useful below and it would not be too hard to add a device that focused any particle with $s > 0$ onto 0.22. Based on Fig. 2 we can see that a particle with $2R = 0.514W$ (○) flowing through the junction corresponds to the fundamental NOT gate. This is because $A = 0$ corresponds to $x_0^* > x$ and to the mapping $0 \mapsto 1$ [Fig. 4(a)], and $A = 1$ corresponds to $x > x_0^*$ and to the mapping $1 \mapsto 0$ [Fig. 4(b)]. The gate exhibits tolerance to both focusing and flow rate errors as both mappings are insensitive to the exact value of s and Q_1/Q_0 at least within $\Delta(s/(W/2)) = \pm 0.01$ and $\Delta(Q_1/Q_0) = \pm 0.025$. Gates could be run in sequence by recombining the two output branches at a later stage.

In the case of two-particle dynamics, the overall propensity of particles to enter the high-flow-rate branch can be turned into binary logic under the assumption that the high-flow-rate branch is allowed to take precedence over the low-flow-rate branch. Namely, we define another binary variable B in terms of the particle separation in the inlet as $B = 0$: $d/R \leqslant 7$, $B = 1$: $d/R \geqslant 10$. The regions associated with different values of B are indicated in Fig. 3(a). We obtain a two-particle NAND gate on the basis that the bifurcation maps the (A,B) pair of variables as $(1,1) \mapsto 0$ [Fig. 4(f)], $(0,0) \mapsto 1$ [Fig. 4(c)], and $(0,1) \mapsto 1$ [Fig. 4(e)] without ambiguity. However, $(A,B) = (1,0)$ [Fig. 4(d)] results in particles going in different directions, for which reason the outcomes $<>$ and $><$ are understood as a binary 1. The exact value $s = 0.22(W/2)$ for $A = 1$ is chosen as it works for $2R = 0.514W$ in both the case of the single-particle NOT gate and the two-particle NAND gate. The latter gate is universal, which in different configurations can realize all other binary gates. Again, gates could be run in sequence by a suitable recombination of the two output branches at a later stage. However, additional focusing may be needed for serial gate configurations. As the device does not rely on instantaneous collisions, e.g., those of water droplets on superphobic surfaces [30], the phase diagram of Fig. 3 and thus the binary operations should exhibit tolerances to focusing error in both quantities d/R and $s/(W/2)$. An increase in particle porosity shifts the phase diagram toward larger values of $s/(W/2)$ and the $\ll$ phase diminishes in size.

Conclusions. Our simulation methodology reproduces quantitatively experimental measurements of solvent and particle flow in T-bifurcations. We have further suggested how particle filtration based on size and porosity is feasible in the T-junction by taking advantage of recently developed, accurate focusing devices. We have predicted that bits of binary information can be encoded into a single focused particle or pairs of particles flowing through the junction.

Acknowledgments. This work was supported by the Academy of Finland through its COMP CoE Grant No. 251748 and by the Natural Science and Engineering Council of Canada. This work was made possible by the facilities of the Shared Hierarchical Academic Research Computing Network (SHARCNET) and Compute/Calcul Canada as well as computational resources provided by the Aalto Science-IT project and CSC, the Finnish IT center for Scientific Computing.

[1] G. Segré and A. Silberberg, Nature (London) **189**, 209 (1961); J. Fluid Mech. **14**, 115 (1962); **14**, 136 (1962).
[2] B. P. Ho and L. G. Leal, J. Fluid Mech. **65**, 365 (1974).
[3] D. Di Carlo, Lab Chip **9**, 3038 (2009).
[4] D. Di Carlo, D. Irimia, R. G. Tompkins, and M. Toner, Proc. Natl. Acad. Sci. USA **104**, 18892 (2007).
[5] A. J. Mach *et al.*, Lab Chip **11**, 2827 (2011).
[6] M. Masaeli *et al.*, Phys. Rev. X **2**, 031017 (2012).
[7] S. Yang, A. Ündar, and J. D. Zahn, Lab Chip **6**, 871 (2006).
[8] R. D. Jäggi, R. Sandoz, and C. S. Effenhauser, Microfluid. Nanofluid. **3**, 47 (2007).
[9] V. Doyeux, T. Podgorski, S. Peponas, M. Ismail, and G. Coupier, J. Fluid Mech. **674**, 359 (2011).
[10] A. J. Chung, D. R. Gossett, and D. Di Carlo, Small **9**, 685 (2012).
[11] K. Svanes and B. W. Zweifach, Microvasc. Res. **1**, 210 (1968).
[12] Y. C. Fung, Microvasc. Res. **5**, 34 (1973).
[13] N. Tsapis, D. Bennett, B. Jackson, D. A. Weitz, and D. A. Edwards, Proc. Natl. Acad. Sci. USA **99**, 12001 (2002).
[14] D. A. Edwards *et al.*, Science **276**, 1868 (1997).
[15] S. T. T. Ollila, T. Ala-Nissila, and C. Denniston, J. Fluid Mech. **709**, 123 (2012).
[16] S. T. T. Ollila, C. Denniston, M. Karttunen, and T. Ala-Nissila, J. Chem. Phys. **134**, 064902 (2011).
[17] S. T. T. Ollila, C. J. Smith, T. Ala-Nissila, and C. Denniston, Multiscale Model. Simul. **11**, 213 (2013).
[18] T. Vestad, D. W. M. Marr, and T. Munakata, Appl. Phys. Lett. **84**, 5074 (2004).
[19] H. C. Brinkman, Appl. Sci. Res. A **1**, 27 (1947).
[20] H. C. Brinkman, Appl. Sci. Res. A **1**, 81 (1947).
[21] P. Debye and A. M. Bueche, J. Chem. Phys. **16**, 573 (1948).

[22] G. C. Abade, B. Cichocki, M. L. Ekiel-Jezewska, G. Nägele, and E. Wajnryb, Phys. Rev. E **81**, 020404(R) (2010).
[23] W. Humphrey, A. Dalke, and K. Schulten, J. Mol. Graphics **14**, 33 (1996).
[24] M. Hecht and J. Harting, J. Stat. Mech. (2010) P01018.
[25] G. S. Kell, J. Chem. Eng. Data **15**, 119 (1970).
[26] S. Chen and G. D. Doolen, Annu. Rev. Fluid Mech. **30**, 329 (1998).
[27] G. K. Batchelor, *An Introduction to Fluid Mechanics* (Cambridge University Press, Cambridge, UK, 1967).
[28] L. D. Landau and E. M. Lifschitz, *Fluid Mechanics*, 2nd ed. (Pergamon, New York, 1987).
[29] C. J. Smith and C. Denniston, J. Appl. Phys. **101**, 014305 (2007).
[30] H. Mertaniemi, R. Forchheimer, O. Ikkala, and R. H. A. Ras, Adv. Mater. **24**, 5738 (2012).